



Photocatalytic degradation of tetracycline on $g\text{-C}_3\text{N}_4\text{@Fe}_3\text{O}_4$ magnetic photocatalyst

Xiaochen Zhao^{a,b}, Shaodong Qu^a, Jichang Han^{a,*}

^aShaanxi Provincial Land Engineering Construction Group, Xi'an 710075, Shaanxi, China. Tel. +86–15102967760; Fax: +86–29–82334566; emails: hanjichang_ge@163.com (J. Han), zxc@xust.edu.cn (X. Zhao), qushaodong@126.com (S. Qu)

^bCollege of Geology and Environment, Xi'an University of Science and Technology, Xi'an 710054, Shaanxi, China

Received 6 August 2018; Accepted 16 December 2018

ABSTRACT

$g\text{-C}_3\text{N}_4\text{@Fe}_3\text{O}_4$ magnetic photocatalyst is prepared by a simple two-steps hydrothermal and chemical adsorption method. The as-prepared samples were characterized by X-ray diffraction, Fourier transform infrared, scanning electron microscopy (SEM), Ultraviolet-visible spectroscopy, and vibrating sample magnetometer. The SEM result shows that Fe_3O_4 nanoparticles dispersed on the $g\text{-C}_3\text{N}_4$ surface and lamellar. The combination of Fe_3O_4 and $g\text{-C}_3\text{N}_4$ can improve the absorption ability of visible light. Meanwhile, the photocatalytic activities were evaluated by the degradation of tetracycline (TC) with visible light. Due to the effective separation of photo-induced electron-hole pairs, $g\text{-C}_3\text{N}_4\text{@Fe}_3\text{O}_4$ a ratio of 3:1 exhibited the best photocatalytic performance, the degradation rate for 120 min on the tetracycline reached 92.84%. In addition, we have found that it has better reusable photocatalyst than other traditional photocatalysts by magnetic separation recycling method.

Keywords: Magnetic photocatalyst; $g\text{-C}_3\text{N}_4$; Fe_3O_4 ; Nanoparticles; Tetracycline

1. Introduction

In recent years, due to the extreme reliance on antibiotics in clinical care and modern aquaculture, the unreasonable use and abuse of antibiotics have become increasingly serious [1,2]. Excessive use of antibiotics will not only damage the organs of humans and livestock, but also induce bacterial drug resistance in organisms [3]. In addition, most of the antibiotics will be excreted in the form of prototypes or metabolites into various water bodies, which not only destroys the water environment, but also threatens the human health since the ecological cycle re-enters the human body [4,5]. Therefore, the efficient removal of antibiotics from water environment has focus researcher's attentions. The emerging photocatalysis technology has many advantages, such as high reactivity, simple operation, no pollution, and fully used solar energy, which provides an efficient, convenient and green way to solve the current water environment pollution problems

[6–8]. Besides, the co-contaminants in raw water could dramatically impact kinetics and reusability of photocatalysts which is very different from those in deionized water [9]. Turbid waters almost always are a challenge to this approach.

Among many photocatalysts, graphite-like carbon nitride ($g\text{-C}_3\text{N}_4$) is favored by scholars for its unique advantages. $g\text{-C}_3\text{N}_4$ is the most stable allotrope among the five crystal forms of carbon nitride at normal temperature, and is an environment-friendly photocatalytic material with low energy gap, high thermal stability, and low preparation cost, which has attracted enthusiastic attention from researchers in recent years [10,11]. Nevertheless, $g\text{-C}_3\text{N}_4$ is limited in practical application due to its low specific surface area, easy composite of photogenerated electron-hole pair, low photogenerated carrier yield and other defects [12,13]. Semiconductor composite contribute to transferring photo-generated electrons from the conduction band of $g\text{-C}_3\text{N}_4$ to other semiconductors, which can prolong the service life of

* Corresponding author.

photogenerated carriers, thus achieving the purpose of effectively improving the photocatalytic performances of g-C₃N₄ [14,15]. However, these composite photocatalytic materials are excessively wasted during sewage treatment due to its good dispersity and hardest recovery. Fe₃O₄ has drawn extensive attention because it has superparamagnetism and is easy to separate magnetically [16,17]. The synthesis of magnetic composite materials such as ZnO/Fe₃O₄ [18] and TiO₂/Fe₃O₄ [19] has shown that the introduction of magnetic materials can effectively improve the recycling rate of raw materials. Meanwhile, Fe₃O₄ has good adsorption, and can provide adsorption sites for organics, so that the photocatalytic effects can be greatly improved.

In this paper, Fe₃O₄ spheres with uniform particle sizes were prepared by hydrothermal method, and g-C₃N₄ was prepared by direct calcination. The g-C₃N₄@Fe₃O₄ magnetic composite photocatalytic material was prepared by chemisorption. The morphology, structure, and performances of the composite material were studied by scanning electron microscopy (SEM), X-ray diffraction (XRD), Fourier transform infrared (FT-IR), vibrating sample magnetometer (VSM), Ultraviolet-visible spectroscopy (UV-vis) technologies, and the effects of the composite ratio of g-C₃N₄ and Fe₃O₄ on the performances of the composite material were investigated. Furthermore, the photocatalytic performances, reaction kinetics and photocatalytic mechanism of as-prepared samples were analyzed with TC as a degradation target under the irradiation of xenon lamp, and the recycling rate of the magnetic material under the effect of external magnetic field was further discussed.

2. Material and methods

2.1. Fabrication of g-C₃N₄@Fe₃O₄

Fabrication of Fe₃O₄: 2.16 g FeCl₃·6H₂O was dissolved in 64 ml glycol reagent, 9.57 g sodium acetate and 1.63 g PEG-4,000 were added into a glycol solution, the mixture was magnetically stirred at room temperature for 1 h and then transferred to a 100 ml polytetrafluoroethylene tank. The polytetrafluoroethylene tank was sealed in a reaction kettle and reacted at 200°C for 12 h. After being cooled at room temperature, the as-prepared black products were respectively washed with deionized water and anhydrous ethanol for several times. The product was dried under vacuum at 60°C to obtain Fe₃O₄ powder.

Fabrication of g-C₃N₄: 2.00 g melamine was added into a sealed crucible, and the crucible was placed in a muffle furnace. The muffle furnace was heated up to 520°C at a rate of 5°C/min and held for 4 h. After the muffle furnace was naturally cooled to room temperature, the yellow product was ground into powder. The powder was dispersed in 200 ml distilled water and ultrasonically processed for 30 min, and then respectively washed with deionized water and anhydrous ethanol for three times. Afterwards, the product was dried at 80°C to obtain g-C₃N₄ powder.

Fabrication of g-C₃N₄@Fe₃O₄: a certain amount of g-C₃N₄ was dispersed in 100 ml methanol solution and ultrasonically processed for 30 min, then 0.10 g Fe₃O₄ and 0.20 g PEG-4,000 were added into the methanol solution above, and the mixture was continuously stirred for 24 h until the methanol

was completely volatilized. The resulting black product was respectively washed with deionized water and anhydrous ethanol for several times. The final product was dried under vacuum at 60°C and ground for standby use. The composite mass ratio of g-C₃N₄ to Fe₃O₄ was 2:1, 3:1, 5:1, and 7:1 respectively.

2.2. Characterization

The crystal structure of the sample was analyzed using a D8 Advance full-automatic XRD from Bruker-AXS in Germany (Cu and K α irradiation, 40 KV, 30 mA, 8°/min scanning speed). The morphology, size, and elemental characteristics of the sample were observed using S-4,800 electron microscope and energy dispersive spectroscopy (EDS) from Hitachi in Japan. Fourier transform infrared spectroscopy (FT-IR) spectrometer (PerkinElmer, Spectrum Two, USA) was applied to obtain FT-IR spectra. Diffused reflectance UV-Vis spectra of the samples were obtained from a UV-Vis spectrophotometer (UV2550, Shimadzu, Japan) from 200–900 nm. The magnetic properties of the material were investigated using a VSM.

2.3. Photocatalytic activity measurement

The photocatalytic performances of the synthesized material were analyzed and compared using a GHX-2 photocatalytic apparatus for TC degradation experiment. The specific operation thereof was as follows: 50 mL of 20 mg/L TC solution was used to dissolve 20 mg of the samples. A 300 W xenon lamp was used as a visible light source, and an optical filter was used to filter ultraviolet rays ($\lambda < 400$ nm). Before visible light irradiation, the solution should be stirred in the dark for 30 min to ensure the adsorption-desorption equilibrium between the photocatalyst and the TC. During irradiation, 3 mL suspension was taken at regular intervals, and then a TC concentration was analyzed using spectrometer after collection and centrifugation, and the absorbance was recorded. The degradation rate of TC is calculated by Eq. (1).

$$\text{Degradation rate (\%)} = (C_0 - C) / C_0 \times 100\% \quad (1)$$

where C_0 was the absorbance achieving system equilibrium after the adsorption in the dark, and C was the absorbance of the TC determined by regular sampling.

3. Results and discussion

3.1. XRD analysis

The structure of as-prepared g-C₃N₄, Fe₃O₄, and g-C₃N₄@Fe₃O₄ (3:1) samples are evaluated by XRD analysis. As shown in Fig. 1, the diffraction peaks at $2\theta = 30.2^\circ, 35.5^\circ, 43.2^\circ, 53.4^\circ, 57.3^\circ,$ and 62.6° in the XRD spectrum of Fe₃O₄ were consistent with JCPDS card No. 82–1533 standard, which indicated that the as-prepared Fe₃O₄ was a pure cubic phase structure. The stronger diffraction peak of the pure g-C₃N₄ at the diffraction angle $2\theta = 27.4^\circ$ coincided with the (002) crystal face of the graphite-like phase g-C₃N₄, which was caused by the stacking of the graphite phase structures [20]. A weaker diffraction peak was observed at $2\theta = 13.1^\circ$, which was corresponding to the (100) crystal face of g-C₃N₄, and formed by the stacking of triazine structural units [21]. The positions of the diffraction peaks of the g-C₃N₄@Fe₃O₄ composite material XRD

were consistent with that of the diffraction peaks of the pure $g\text{-C}_3\text{N}_4$, and no obvious displacement phenomenon were found, which indicated that the introduction of nano- Fe_3O_4 did not change the crystal form of $g\text{-C}_3\text{N}_4$. It could also be observed from the figure that the characteristic peak of $g\text{-C}_3\text{N}_4$ was weakened at $2\theta = 27.4^\circ$ because the introduction of Fe_3O_4 suppressed the stacking of the (002) crystal face of $g\text{-C}_3\text{N}_4$ in a vertical direction, which was beneficial for enhancing the dispersity and specific surface area of $g\text{-C}_3\text{N}_4$, and further improving the photocatalytic activity of $g\text{-C}_3\text{N}_4$. In the XRD spectrum of the $g\text{-C}_3\text{N}_4/\text{Fe}_3\text{O}_4$ composite material, the characteristic peaks of $g\text{-C}_3\text{N}_4$ and Fe_3O_4 coexisted, indicating that no other impurities appeared in the as-prepared composite material.

3.2. FT-IR analysis

The chemical structure of the $g\text{-C}_3\text{N}_4/\text{Fe}_3\text{O}_4$ composite material was further analyzed using FT-IR spectroscopy, and the results were shown in Fig. 2. In Fig. 2(f) pure Fe_3O_4

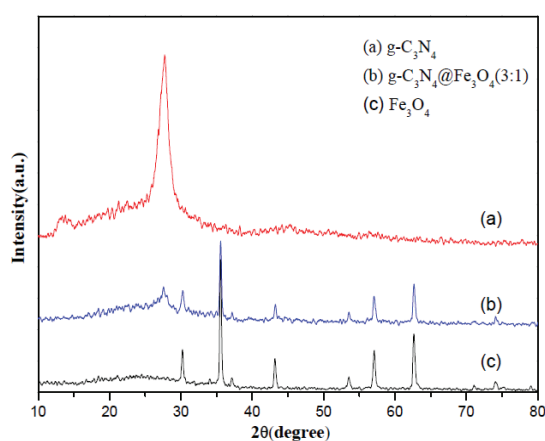


Fig. 1. XRD patterns for pure $g\text{-C}_3\text{N}_4$, pure Fe_3O_4 , and $g\text{-C}_3\text{N}_4/\text{Fe}_3\text{O}_4$.

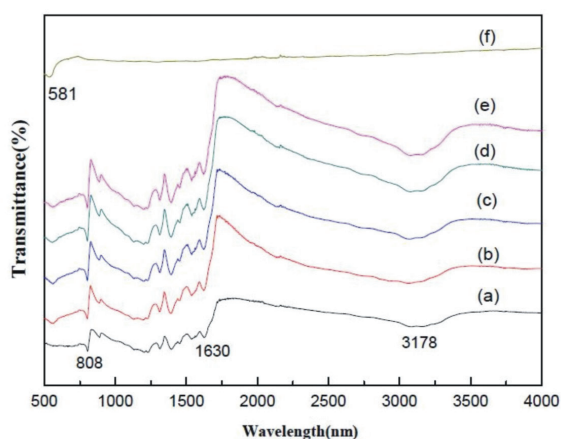


Fig. 2. FT-IR spectra of (a) $g\text{-C}_3\text{N}_4$, (b) $g\text{-C}_3\text{N}_4/\text{Fe}_3\text{O}_4$ (2:1), (c) $g\text{-C}_3\text{N}_4/\text{Fe}_3\text{O}_4$ (3:1), (d) $g\text{-C}_3\text{N}_4/\text{Fe}_3\text{O}_4$ (5:1), (e) $g\text{-C}_3\text{N}_4/\text{Fe}_3\text{O}_4$ (7:1) and (f) Fe_3O_4 .

was corresponding to the characteristic absorption peak of Fe-O bond at 581 cm^{-1} [22]. The characteristic peak of the pure $g\text{-C}_3\text{N}_4$ mainly appeared in three regions including 808 , $1,200\text{--}1,650$, and $3,100\text{--}3,300\text{ cm}^{-1}$. The absorption peak at 808 cm^{-1} was corresponding to the bending vibration absorption of $g\text{-C}_3\text{N}_4$ triazine aromatic ring structure molecules. A plurality of absorption peaks appeared in the region of $1,200$ to $1,650\text{ cm}^{-1}$, corresponding to the stretching vibration characteristic peaks of CN heterocycle and C-N bond. The wider characteristic absorption peaks at $3,100$ to $3,300\text{ cm}^{-1}$ were caused by the stretching vibration of N-H bond and O-H vibration mode that absorbs moisture on the surface, which indicated that there were products incompletely polycondensed by direct calcination of melamine, and N-H bond existed at the layered edge of $g\text{-C}_3\text{N}_4$ [23]. It could be concluded from the spectrum of Figs. 2(e)-(b) that in the $g\text{-C}_3\text{N}_4/\text{Fe}_3\text{O}_4$ composite material, the characteristic peak strength of Fe_3O_4 was improved with the increasingly loaded Fe_3O_4 , and all characteristic peaks of $g\text{-C}_3\text{N}_4$ appeared were slightly changed, which indicated that the composite of two phase materials of Fe_3O_4 and $g\text{-C}_3\text{N}_4$ was not only a simple physical effect, and other close interactions may exist between the interfaces [23].

3.3. Scanning electron microscope

Fig. 3 shows morphologic diagram of the as-prepared $g\text{-C}_3\text{N}_4$, Fe_3O_4 and $g\text{-C}_3\text{N}_4/\text{Fe}_3\text{O}_4$ observed by scanning electron microscope (SEM). As shown in Fig. 3(a), Fe_3O_4 prepared by solvothermal reaction was a sphere with a diameter of 200 nm , and had the characteristics of uniform morphology, uniform size, and good dispersity. It could be clearly observed from Fig. 3(b) that the overall morphology of $g\text{-C}_3\text{N}_4$ was an irregular block structure, and the block was formed by stacking thin laminated structures of different sizes. The morphologic diagram of the $g\text{-C}_3\text{N}_4/\text{Fe}_3\text{O}_4$ composite material is shown in Fig. 3(c), the Fe_3O_4 spheres were evenly dispersed on the surface of $g\text{-C}_3\text{N}_4$. Fig. 3(d) is a three-fold larger version of Fig. 3(c), it could be observed from the side that partial Fe_3O_4 was interspersed between the laminated structures of $g\text{-C}_3\text{N}_4$, resulting in the increase of spacing between the laminated structures, so that the surface area of $g\text{-C}_3\text{N}_4$ was increased, which was beneficial for improving the photocatalytic effect of the composite material, and this was consistent with the result of XRD analysis.

3.4. Uv-vis

Fig. 4 shows the UV-vis diffuser reflectance spectrum of pure $g\text{-C}_3\text{N}_4$ and Fe_3O_4 , and the $g\text{-C}_3\text{N}_4/\text{Fe}_3\text{O}_4$ composite materials with different Fe_3O_4 contents. Fig. 4(a) shows the light absorption of the pure $g\text{-C}_3\text{N}_4$ in the wave band ranging from 300 to 700 nm , and $g\text{-C}_3\text{N}_4$ exhibited a strong light absorptivity near the wavelength of 460 nm . Compared with the pure $g\text{-C}_3\text{N}_4$, Fe_3O_4 exhibited a wide light absorption range, which may be related to its own black color. After $g\text{-C}_3\text{N}_4$ and Fe_3O_4 were composited, the visible light absorption range of the composite material was significantly expanded, the absorption peak of the $g\text{-C}_3\text{N}_4/\text{Fe}_3\text{O}_4$ composite was obviously red-shifted and had stronger absorption to the visible light in the wave band ranging from 400 to 700 nm , and this

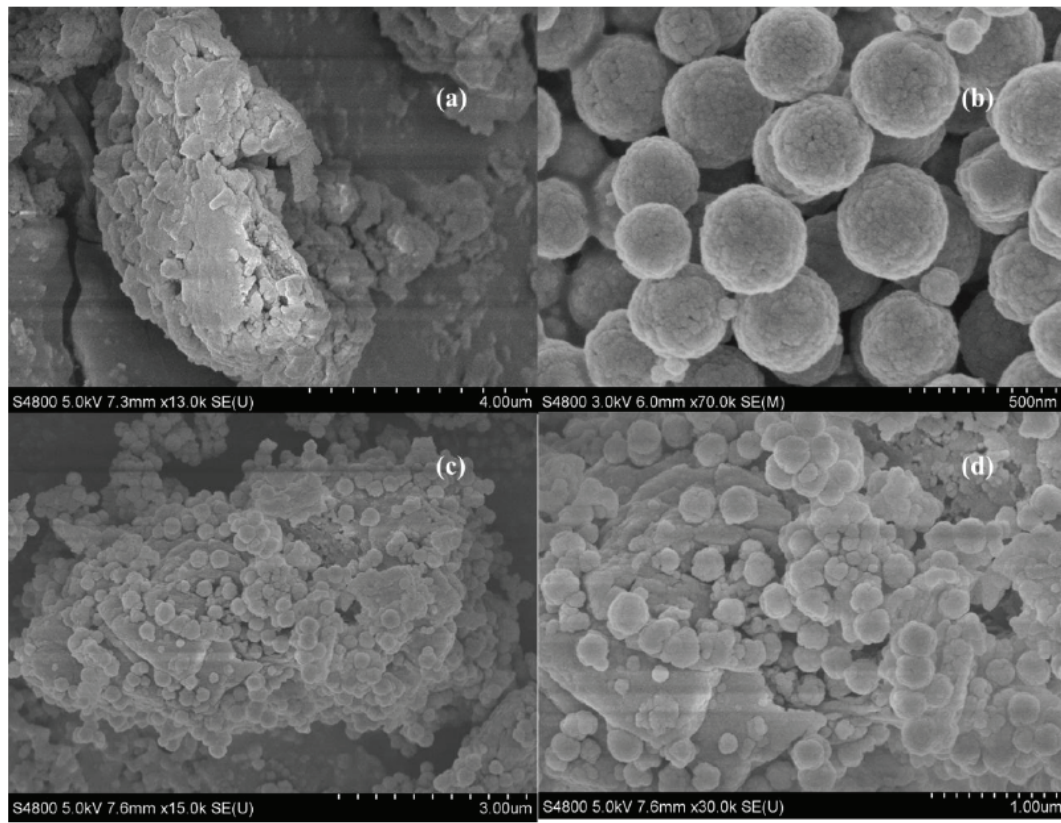


Fig. 3. SEM images of (a) g-C₃N₄, (b) Fe₃O₄ and (c) g-C₃N₄@Fe₃O₄(3:1).

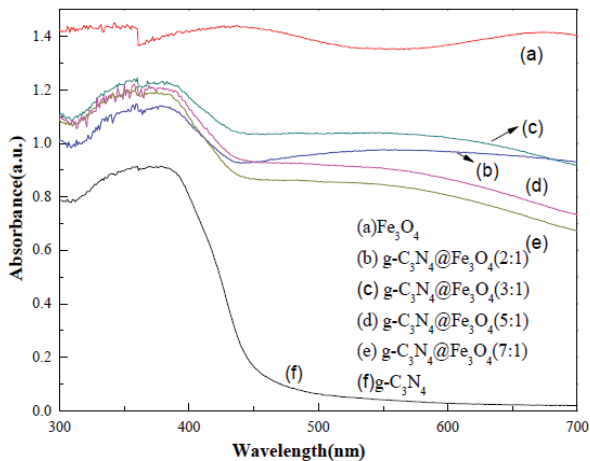


Fig. 4. UV-vis diffuse reflectance spectra of different samples.

result showed that the composite of Fe₃O₄ promoted the visible light absorption of g-C₃N₄. It is worth noting that it could be observed from Figs. 4(b), (e) that the visible light absorption range of the product was increased with the increasingly loaded Fe₃O₄; however, when the ratio of g-C₃N₄ to Fe₃O₄ was greater than 3:1, the response of the composite material to the visible light was significantly reduced. This might be caused by the competition between Fe₃O₄ and g-C₃N₄ for visible light absorption, and excessive Fe₃O₄ loaded on the surface of

g-C₃N₄ could suppress the utilization of the visible light by g-C₃N₄, thus reducing the photocatalytic activity of g-C₃N₄ [24]. The response of the composite material to the visible light was related to the new energy band structure formed by the as-prepared composite photocatalyst and the tensile strain generated by the difference of lattices between two phases. In summary, it could be concluded that the appropriate composite ratio of Fe₃O₄ to g-C₃N₄ helped enhance the visible light absorption, thereby promoting the product to produce more electron-hole pairs by fully utilizing the visible light during the photocatalytic reaction, so as to improve the photocatalytic activity.

3.5. VSM characteristics

Fig. 5 shows the magnetic properties of the pure Fe₃O₄ and the g-C₃N₄@Fe₃O₄ composite materials prepared by different raw material ratios at room temperature. It could be known from Fig. 5(a) that the saturation magnetic moment of Fe₃O₄ nanoparticles obtained at room temperature was 106.75 emu/g, indicated that the as-prepared Fe₃O₄ had strong ferromagnetism. The g-C₃N₄@Fe₃O₄ composite photocatalyst prepared by chemisorption exhibited a certain magnetic force. With the increase of the Fe₃O₄ added, the saturation magnetic value of the composite material was gradually increased, as shown in Figs. 5(b)–(e). When the composite ratio of g-C₃N₄ to Fe₃O₄ was 3:1, the saturation force moment of g-C₃N₄@Fe₃O₄ at room temperature was 22.28 emu/g, exhibiting a very strong ferromagnetic behavior. To further

verify the magnetization properties of the composite material, a certain amount of sample was dispersed in a tetracycline solution. Fig. 5(f) shows the separation and contrast effects of the sample under the action of an external magnetic field after the tetracycline solution was degraded. It could be clearly seen that the $g\text{-C}_3\text{N}_4/\text{Fe}_3\text{O}_4$ composite material could be completely attracted under the action of the external magnetic field, which indicated that the as-prepared $g\text{-C}_3\text{N}_4/\text{Fe}_3\text{O}_4$ composite material had a very strong magnetic property and was beneficial to the separation and recycling of the composite photocatalyst during practical utilization.

3.6. Photocatalytic performance

According to the discussion and analysis above, it was known that $g\text{-C}_3\text{N}_4/\text{Fe}_3\text{O}_4$ prepared by chemisorption had excellent theoretical properties. To further verify the photocatalytic activity of the composite material in practical application, the experiment aimed to degrade tetracycline, and at the maximum absorption wavelength of 356 nm, the photocatalytic effects of the pure $g\text{-C}_3\text{N}_4$ and the $g\text{-C}_3\text{N}_4/\text{Fe}_3\text{O}_4$ materials synthesized according to different ratios were investigated. As shown in Fig. 6(a), the pure-phase $g\text{-C}_3\text{N}_4$ exhibited a lower photocatalytic activity, and only 62.94% of the TC was degraded after light irradiation for 120 min. In contrast, the photocatalytic effect of the material showed a qualitative leap after loading Fe_3O_4 on $g\text{-C}_3\text{N}_4$. With the increasingly loaded Fe_3O_4 , the degradation rate of tetracycline was increased gradually, and the photocatalytic activity of $g\text{-C}_3\text{N}_4/\text{Fe}_3\text{O}_4$ became more and more obvious. When the ratio of $g\text{-C}_3\text{N}_4$ to Fe_3O_4 was 3:1, the degradation rate of the $g\text{-C}_3\text{N}_4/\text{Fe}_3\text{O}_4$ after light irradiation for 120 min on the tetracycline reached 92.84%, which showed the best photocatalytic effect. Because Fe_3O_4 had a narrow band gap (0.1 eV) and good electrical conductivity ($1.9 \times 10^6 \text{ Sm}^{-1}$), it could serve as a medium to rapidly transfer the photogenerated electrons, thus effectively reducing the composite rate of $g\text{-C}_3\text{N}_4$ photogenerated electron-hole pair, and thus helping to improve the photocatalytic activity of $g\text{-C}_3\text{N}_4$ [25]. However, when the ratio of raw materials was continuously increased, the photocatalytic activity was significantly decreased. This was

mainly due to the presence of a large amount of Fe_3O_4 on the surface of $g\text{-C}_3\text{N}_4$. Fe_3O_4 could serve as a composite center of electrons and holes, resulting in a decrease in the photocatalytic activity of the composite. This was consistent with the UV-vis characterization results [26].

Fig. 7 is a pseudo-first order reaction kinetics fitting result of the photocatalytic degradation of the as-prepared sample on a tetracycline solution. The photocatalytic degradation of the composite material on the tetracycline molecules was in conformity with to a first-order reaction kinetic equation: $-\ln(C_t/C_0) = k \cdot t$. Where C_t denoted the concentration of the TC solution at the time t in the photocatalytic reaction, C_0 denoted the concentration of the TC solution at the beginning of the photocatalytic reaction, and k was a reaction rate constant.

As shown in Fig. 7, during the photocatalytic degradation of the TC by the $g\text{-C}_3\text{N}_4/\text{Fe}_3\text{O}_4$ composite materials prepared with different ratios. As shown in Table 1, the k of the pure $g\text{-C}_3\text{N}_4$ was 0.0089 min^{-1} . However, the reaction rate constant k was 0.0198 min^{-1} when the raw material ratio was 3:1, which was about 2.2 times that of the pure $g\text{-C}_3\text{N}_4$, showing the best

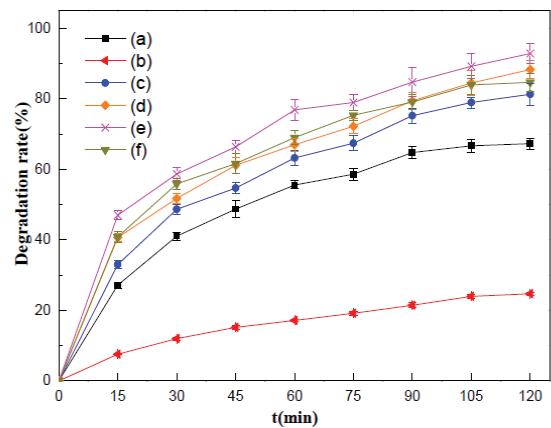


Fig. 6. Photodegradation of TC solution under (a) $g\text{-C}_3\text{N}_4$, (b) Fe_3O_4 , (c) $g\text{-C}_3\text{N}_4/\text{Fe}_3\text{O}_4$ (7:1), (d) $g\text{-C}_3\text{N}_4/\text{Fe}_3\text{O}_4$ (5:1), (e) $g\text{-C}_3\text{N}_4/\text{Fe}_3\text{O}_4$ (3:1) and (f) $g\text{-C}_3\text{N}_4/\text{Fe}_3\text{O}_4$ (2:1).

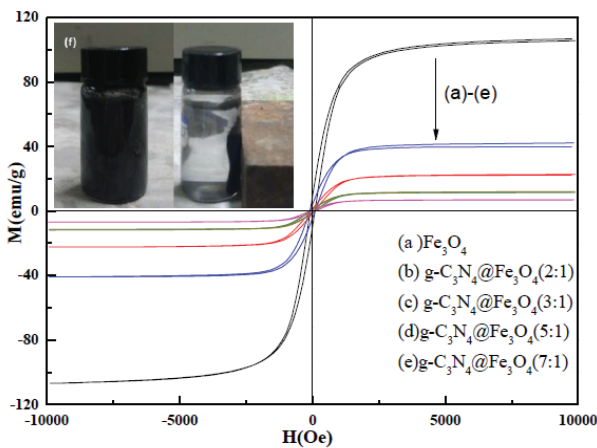


Fig. 5. Magnetization-hysteresis curve of different samples.

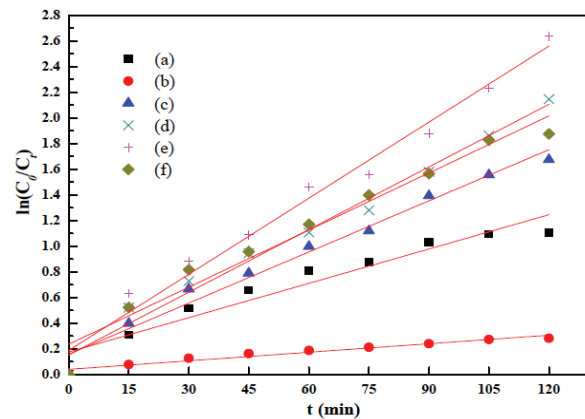


Fig. 7. Photodegradation kinetics of TC solution in (a) $g\text{-C}_3\text{N}_4$, (b) Fe_3O_4 , (c) $g\text{-C}_3\text{N}_4/\text{Fe}_3\text{O}_4$ (7:1), (d) $g\text{-C}_3\text{N}_4/\text{Fe}_3\text{O}_4$ (5:1), (e) $g\text{-C}_3\text{N}_4/\text{Fe}_3\text{O}_4$ (3:1) and (f) $g\text{-C}_3\text{N}_4/\text{Fe}_3\text{O}_4$ (2:1).

Table 1
Value k and R^2 of different samples

Sample	7:1	5:1	3:1	2:1	Fe ₃ O ₄	g-C ₃ N ₄
k (min ⁻¹)	0.013	0.016	0.020	0.015	0.002	0.009
R^2	0.976	0.980	0.978	0.960	0.944	0.924

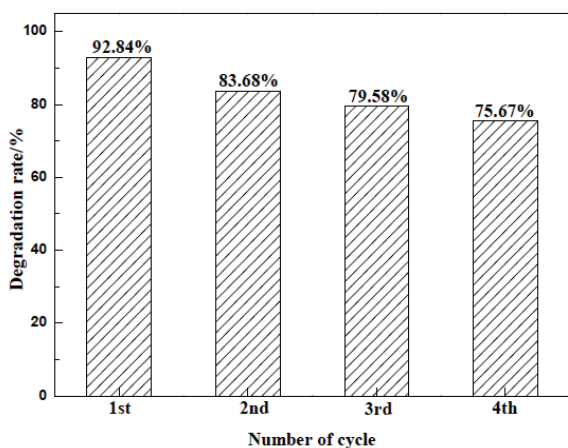


Fig. 8. Recyclability of g-C₃N₄@Fe₃O₄ composites degrading on TC.

photocatalytic effect. It indicated that the photocatalytic activity of the composite material was greatly improved. The reason could be known from the analysis results of the UV diffuser reflection. In addition, Fe₃O₄ could not only enlarge the visible light absorption range of g-C₃N₄, but also provide adsorption sites for organic adsorption, thereby improving the photocatalytic degradation efficiency of g-C₃N₄.

3.7. Stability and reusability

In recent years, the stability and reusability of the photocatalyst have become the focus of attention. Therefore, the recovery and reuse experiments were used to evaluate the potential of the composite materials in practical application. An external magnetic field force was used to separate, wash, and collect the catalyzed and degraded g-C₃N₄@Fe₃O₄ photocatalyst with a ratio of 3:1, and then photocatalytic degradation was repeated. The results are shown in Fig. 8. After 4 cycles, the g-C₃N₄@Fe₃O₄ material with a ratio of 3:1 still exhibited a higher catalytic activity, and after light irradiation for 120 min, there was still 75.67% of the TC could be removed. Thus it could be seen that the g-C₃N₄@Fe₃O₄ composite photocatalyst still had a certain photocatalytic activity after being repeatedly used for many times. Therefore, the magnetic composite photocatalyst had good stability and could be repeatedly used for many times in practical application.

4. Conclusions

In this paper, Fe₃O₄ nanospheres were successfully prepared by solvothermal method. The g-C₃N₄@Fe₃O₄ composite was prepared by adsorption self-assembly and directly calcinations. The structure, morphology, magnetic, and photoreponse characteristics of the photocatalyst formed by g-C₃N₄

and Fe₃O₄ with different ratios were studied by XRD, FT-IR, SEM, UV-vis, VSM. The results showed that the Fe₃O₄ nanospheres were uniformly dispersed on the surface of g-C₃N₄, which contributed to the effective separation of the photo-generated electron-hole pair. When the ratio of g-C₃N₄ to Fe₃O₄ was 3:1, the materials showed the best photocatalytic activity. In addition, the g-C₃N₄@Fe₃O₄ composites showed very strong magnetic property, which had wide applicability in removing the TC from water, and provided an effective way to solve the problem of secondary pollution caused by good dispersibility and difficult recovery of the g-C₃N₄ photocatalyst.

Acknowledgements

This study was supported by the ministry of land and resources' key laboratory opening fund for degradation and unused land remediation projects (No. SXDJ2018-09).

References

- [1] Q. Bu, B. Wang, J. Huang, S. Deng, G. Yu, Pharmaceuticals and personal care products in the aquatic environment in China: a review, *J. Hazard. Mater.*, 262 (2013) 189–211.
- [2] M. Topal, T. E. I. Arslan, Occurrence and fate of tetracycline and degradation products in municipal biological wastewater treatment plant and transport of them in surface water, *Environ. Monit. Assess.*, 187 (2015) 750.
- [3] C.Y. Lu, J.J. Dang, C. T. Hou, Y.J. Jiang, W. S. Guan, Photocatalytic degradation of doxycycline on ellipsoid-like BiVO₄ synthesized by EDTA-assisted. *Desal. Wat. Treat.*, 104 (2018) 250–256.
- [4] C. Li, G. Chen, J. Sun, J. Rao, Z. Han, Y. Hu, W. Xing, C. Zhang., Doping effect of phosphate in Bi₂WO₆ and universal improved photocatalytic activity for removing various pollutants in water, *Appl. Catal. B-Environ.*, 188 (2016) 39–47.
- [5] C. Y. Lu, W. S. Guan, T. K. A. Hoang, J. F. Guo, H. G. Gou, Y. L. Yao, Visible-light-driven catalytic degradation of ciprofloxacin on metal (Fe, Co, Ni) doped titanate nanotubes synthesized by one-pot approach, *J. Mater. Sci-Mater. El.*, 27 (2016) 1966–1973.
- [6] R. M. Mohamed, I. A. Mkhallid, M. Abdel Salam, M. A. Barakat, Zeolite Y from rice husk ash encapsulated with Ag-TiO₂: characterization and applications for photocatalytic degradation catalysts, *Desal. Wat. Treat.*, 51 (2013) 7562–7569.
- [7] Z. Zhu, X. Tang, C. Ma, M. Song, N. Gao, Y. Wang, P. Huo, Z. Lu, Y. Yang, Fabrication of conductive and high-dispersed Ppy@Ag/g-C₃N₄ composite photocatalysts for removing various pollutants in water, *Appl. Surf. Sci.*, 387 (2016) 366–374.
- [8] C. Li, S. Yu, H. Dong, C. Liu, H. Wu, H. Che, G. Chen, Z-scheme mesoporous photocatalyst constructed by modification of Sn₃O₄ nanoclusters on g-C₃N₄ nanosheets with improved photocatalytic performance and mechanism insight, *Appl. Catal. B-Environ.*, 238 (2018) 284–293.
- [9] M. Topal, Gülşad Uslu Şenel, E. Öbek, E. Işıl Arslan Topal, Investigation of relationships between removals of tetracycline and degradation products and physicochemical parameters in municipal wastewater treatment plant, *J. Environ. Manage.*, 173 (2016) 1–9.
- [10] Y. Wang, X. C. Wang, M. Antonietti, Polymeric graphitic carbon nitride as a heterogeneous organocatalyst: from photochemistry to multipurpose catalysis to sustainable chemistry, *Angew. Chem. Int. Ed.*, 51 (2012) 68–89.
- [11] Z. Zhu, W. Fan, Z. Liu, H. Dong, Y. Yan, P. Huo, Construction of an attapulgite intercalated mesoporous g-C₃N₄ with enhanced photocatalytic activity for antibiotic degradation, *J. Photochem. Photobiol. A.*, 359 (2018) 102–110.
- [12] C. Ye, J.X. Li, Z.J. Li, X.B. Li, X.B. Fan, L.P. Zhang, B. Chen, C.H. Tung, L.Z. Wu, Enhanced driving force and charge separation efficiency of protonated g-C₃N₄ for photocatalytic O₂ evolution, *ACS Catal.*, 5 (2015) 6973–6979.

- [13] S. Zhang, J. Li, X. Wang, Y. Huang, M. Zeng, J. Xu, Rationally designed 1D Ag@AgVO₃ nanowire/graphene/protonated g-C₃N₄ nanosheet heterojunctions for enhanced photocatalysis via electrostatic self-assembly and photochemical reduction methods, *J. Mater. Chem. A*, 3 (2015) 10119–10126.
- [14] L. M. Sun, X. Zhao, C. J. Jia, Y. X. Zhou, X. F. Cheng, P. Li, Li Liub, W. L. Fan, Enhanced visible-light photocatalytic activity of g-C₃N₄-ZnWO₄ by fabricating a heterojunction: investigation based on experimental and theoretical studies, *J. Mater. Chem.*, 22 (2012) 23428–23438.
- [15] L.Y. Huang, Y.P. Li, H. Xu, Y.G. Xu, J.X. Xia, K. Wang, H.M. Li, X. N. Cheng, Synthesis and characterization of CeO₂/g-C₃N₄ composites with enhanced visible-light photocatalytic activity, *RSC Adv.*, 3 (2013) 22269–22279.
- [16] A. Anise, A. Habibi-Yangjeh, Novel magnetically separable g-C₃N₄/AgBr/Fe₃O₄ nanocomposites as visible-light-driven photocatalysts with highly enhanced activities, *Ceram. Int.*, 41(2015) 5634–5643.
- [17] Z. Zhu, X. Tang, S. Kang, P. Huo, M. Song, W. Shi, Z. Lu, Y. Yang, Constructing of the magnetic photocatalytic nanoreactor MS@FCN for cascade catalytic degrading of tetracycline, *J. Phys. Chem. C*, 120 (2016) 27250–27258.
- [18] V. C. Nguyen, Bifunctional core-shell nanocomposite Mn-doped ZnO/Fe₃O₄ for photodegradation of reactive blue 198 dye, *Adv. Nat. Sci-Nanosci.*, 5 (2014) 035014.
- [19] A. Banisharif, S.H. Elahi, A.A. Firooz, A.A. Khodadadi, Y. Mortazavi, TiO₂/Fe₃O₄ nanocomposite photocatalysts for enhanced photo-decolorization of congo red dye, *Value. Health.*, 15 (2013) 4–5.
- [20] C. Li, S. Yu, H. Dong, Y. Wang, H. Wu, X. Zhang, G. Chen, C. Liu, Mesoporous ferriferrous oxide nanoreactors modified on graphitic carbon nitride towards improvement of physical, photoelectrochemical properties and photocatalytic performance, *J. Colloid. Interf. Sci.*, 531 (2018) 331–342.
- [21] P. Suyana, N. Priyanka Ganguly, Nair, A.M. Peer, K. G. K. Warrior. Co₃O₄-C₃N₄ p-n nano-heterojunctions for the simultaneous degradation of a mixture of pollutants under solar irradiation, *Environ. Sci-Nano.*, 4 (2017) 212–221.
- [22] S. Yang, Y. Gong, J. Zhang, L. Zhan, L. Ma, Z. Fang, R. Vajtai, X. Wang, P. M. Ajayan, Exfoliated graphitic carbon nitride nanosheets as efficient catalysts for hydrogen evolution under visible light, *Adv. Mater.*, 25(2013) 2452–2456.
- [23] X. G. Yu, J. Q. Wan, Y. Shan, K. Chen, X. Han, A facile approach to fabrication of bifunctional magnetic-optical Fe₃O₄@ZnS microspheres, *Chem. Mater.*, 21(2009) 4892–4898.
- [24] Y.L. Chen, J.H. Li, Z.H. Hong, B. Shen, B. Lin, B. Gao, Origin of the enhanced visible-light photocatalytic activity of CNT modified g-C₃N₄ for H₂ production, *Phys. Chem. Chem. Phys.*, 16 (2014) 8106–8113.
- [25] S. Huang, Y. Xu, M. Xie, H. Xu, M. Q. He, J.X. Xia, L.Y. Huang, H.M. Lia, Synthesis of magnetic CoFe₂O₄/g-C₃N₄ composite and its enhancement of photocatalytic ability under visible-light, *Colloids. Surf., A*, 478 (2015) 71–80.
- [26] S. Kumar, T. Surendar, B. Kumar, A. Baruah, V. Shanker. Synthesis of magnetically separable and recyclable g-C₃N₄-Fe₃O₄ hybrid nanocomposites with enhanced photocatalytic performance under visible-light irradiation, *J. Phys. Chem. C*, 117 (2013) 26135–26143.